THE ASTROPHYSICAL JOURNAL, 462:255–265, 1996 May 1

DEEP INFRARED ARRAY IMAGING OF GLOBULAR CLUSTERS. IV. M22 (NGC 6656)

T. J. DAVIDGE[1]
Canadian Gemini Project Office, Dominion Astrophysical Observatory, 5071 W Saanich Road, Victoria, BC, Canada V8X 4M6;[2] and Department of Geophysics and Astronomy, University of British Columbia, Vancouver, BC, Canada V6T 1Z4; davidge@dao.nrc.ca

AND

W. E. HARRIS[1]
Department of Physics and Astronomy, McMaster University, Hamilton, Ontario, Canada L8S 4M1; harris@physics.mcmaster.ca
Received 1995 October 2; accepted 1995 November 7

ABSTRACT

Moderately deep J and K' images, recorded during subarcsecond seeing conditions, are used to investigate the near-infrared color-magnitude diagram (CMD) of the heavily reddened metal-poor globular cluster M22 (NGC 6656). The CMD constructed from these data extends from $K = 7$ to $K = 18$, and includes the upper portions of the main sequence. The main-sequence turnoff (MSTO) occurs at $K = 15.1$ and $J-K = 0.41$—values that are well matched by metal-poor 12 Gyr isochrones from Bergbusch & VandenBerg and Straniero & Chieffi after adopting canonical values for the cluster distance and reddening. For comparison, 16 Gyr isochrones are unable to match the brightness and color of the MSTO, although we emphasize that uncertainties in our current knowledge of stellar structure and evolution make any estimate of absolute ages tentative. We also compare the M22 CMD with that obtained for M13 by Davidge & Harris. After correcting for differences in distance, reddening, and [Fe/H], we find that the brightnesses of the subgiant branch (SGB) and MSTO in M22 and M13 are not significantly different. However, the M22 giant branch is steeper than that in M13, a finding contrary to the relative metallicities of these clusters, but consistent with earlier optical observations by Hesser, Hartwick, & McClure. In particular, the lower giant branch of M22 falls blueward of M13, although the upper giant branches coincide. We suggest that the overall giant branch slope at near-infrared wavelengths may be sensitive to parameters other than age and [Fe/H]. Finally, we investigate the mass function of stars with masses between 0.5 and 0.8 $M_\odot$. The data are consistent with a relatively flat mass function above 0.6 $M_\odot$, a result broadly consistent with what would be predicted based on the mean metallicity and location of M22 in the Galaxy.

Subject headings: globular clusters: individual (M22) — infrared: stars — stars: evolution — stars: luminosity function, mass function

1. INTRODUCTION

A large number of globular clusters are viewed along lines of sight that pass through the Galactic disk and bulge. These clusters are potentially of great interest for studies of Galactic evolution, as they provide a fossil record of conditions in the central regions of the proto-Galaxy. Unfortunately, fundamental parameters such as age, metallicity, and distance remain highly uncertain for many of these clusters, due to complications introduced by differential reddening and field star contamination, both of which introduce scatter in color-magnitude diagrams (CMDs) at optical wavelengths.

M22 (NGC 6656) is one example of how our knowledge of even the nearest low-latitude globular clusters can be compromised by differential reddening and field star contamination. Only a limited number of photometric investigations have been attempted of M22, even though the cluster has a distance of only 2.6 kpc (Peterson & Cudworth 1994). Arp & Melbourne (1959), Lloyd Evans (1975), and Alcaino (1977) used multicolor photographic observations to construct CMDs of the brightest giants in M22. Although containing a large amount of scatter, these CMDs reveal a steep giant branch indicative of a low metallicity. Using photoelectric measurements, Hesser, Hartwick, & McClure (1977) concluded that the CMD of M22 is anomalous, in that the giant branch has a shallower slope than would otherwise be expected based on other metallicity indicators. Alcaino & Liller (1983) and Samus et al. (1995) used photographic data to measure the approximate brightness and color of the main-sequence turnoff (MSTO), but in both cases the MSTO falls near the limits of the photometry, and the scatter in these data makes a credible age determination difficult. More recently, Peterson & Cudworth (1994) used photographic data to measure proper motions and identify cluster members. The giant branch in the resulting CMD shows a dispersion of roughly ± 0.15 mag in $B-V$.

The only photometric study of M22 based on CCD data is that by Anthony-Twarog, Twarog, & Craig (1995), who recorded images of three cluster fields in the *uvby* Ca system. The resulting CMD extends roughly 2 mag below the horizontal branch (HB). The dispersion about the red giant branch (RGB) locus suggests that differential reddening may not be as large as once thought, amounting to $\Delta E(B-V) \sim 0.08$. However, even this relatively modest variation in $E(B-V)$ contributes almost 0.25 mag scatter in V, which in turn introduces considerable uncertainty when measuring the brightness of, for example, the HB and MSTO.

[1] Visiting Astronomer, Canada-France-Hawaii Telescope, which is operated by the National Research Council of Canada, the Centre National de la Recherche Scientifique de France, and the University of Hawaii.
[2] Postal address.

A property of M22 that has drawn considerable attention in the past is the range of chemical abundances seen among the brightest giants (e.g., Hesser, Hartwick, & McClure 1976; Norris & Freeman 1983). It goes without saying that cluster membership is of critical importance when assessing the significance of this effect (Lloyd Evans 1978). Nevertheless, even after considering field star contamination, the range in C and N strengths appears to be substantial, amount to roughly 1 dex (Brown, Wallerstein, & Oke 1990), and comparable variations may be present among other elements, such as Ca (Anthony-Twarog et al. 1995). The origin of this chemical composition dispersion remains a matter of active debate. The relative abundances of ^{12}C and ^{13}C suggest that giants in M22 experienced mixing (e.g., Smith & Suntzeff 1989); however, there are also indications that the observed CN abundance variations may be primordial in origin. For example, the abundances of Ca, Na, and Fe—elements that are produced only in the most advanced stages of evolution in massive stars—appear to be related to CN strength (Wallerstein, Leep, & Oke 1987; Lehnert, Bell, & Cohen 1991; Brown & Wallerstein 1992; Anthony-Twarog et al. 1995). Moreover, the combined C + N + O abundance in M22 giants is not uniform from star to star (Brown et al. 1990), in contrast to what would be expected if mixing were the sole cause of the abundance peculiarities. Finally, abundance variations are detected in giants near the base of the RGB, so that if mixing is the cause of the observed chemical dispersion, then it must occur early in the post–main-sequence evolutionary phase (Anthony-Twarog et al. 1995). These points notwithstanding, Langer, Hoffman, & Sneden (1993) maintain that at least some of the abundance correlations seen among M22 giants may not be primordial in origin.

Clearly, it is of interest to measure the age of M22, especially with respect to other globular clusters, as this may provide clues about the early star-forming history within the solar circle, and the origins of abundance peculiarities. Age determinations require photometry of stars near the MSTO, and, for clusters at low Galactic latitudes, studies of this nature are best done in the near-infrared, where the decreased sensitivity to reddening and reddening variations, coupled with the tendency for atmospheric seeing to improve toward longer wavelengths (Fried 1966), makes it possible to obtain photometry of main-sequence stars that can only be studied with difficulty at optical wavelengths. In the current paper, which is the fourth in a series describing deep near-infrared imaging of globular clusters, we discuss J and K' images of four fields in and around M22. Details of the observations and data reduction are given in § 2. A composite (K, $J-K$) CMD, which is the first at any wavelength to sample stars in M22 fainter than the MSTO, is presented in § 3. In §§ 4 and 5 we compare the ridgeline of the near-infrared CMD to that of metal-poor isochrones and the cluster M13 (Davidge & Harris 1995, hereafter Paper III), which spectroscopic observations indicate has a mean metallicity similar to M22. The mass function of M22 is investigated in § 6, while a brief summary of our results follows in § 7.

2. OBSERVATIONS AND DATA REDUCTION

The data were obtained during the nights of UT 1993 August 29 and 30 with the REDEYE near-infrared imager, which was mounted at the f/8 focus of the 3.6 m Canada-France-Hawaii Telescope (CFHT). The REDEYE detector is a 256 × 256 Hg:Cd:Te array with 40 μm square pixels; a detailed description of the instrument has been given by Simons et al. (1993). The narrow field optics were installed, which resulted in a spatial scale of 0.2 arcsec pixel^{-1} and a total field of view of 51 × 51″. The telescope pointing was offset by a few arcseconds between successive exposures of each field (i.e., "dithering") to facilitate the suppression of bad pixels and the construction of sky flats, with the results that the final processed images cover a smaller field than the raw data.

Images were recorded through K' (Wainscoat & Cowie 1992) and Caltech-CTIO J filters. A total of four fields, of which three sample the cluster proper while a fourth covers the surrounding background, were observed, and an observing log is given in Table 1. Field 1 was observed with two integration times in order to cover the large range of giant-branch stars seen near the cluster center. A number of photometric standard stars from the list published by Casali & Hawarden (1992) were also observed; details of the transformation into the standard system can be found in Paper III.

The procedures used to reduce the M22 data closely follow those described in earlier papers of this series. In summary, the steps involved in the data reduction were as follows: (1) subtraction of a median dark frame from each raw image; (2) division of the result by sky flats; (3) removal of the mean sky level from each flat-fielded frame; (4) registration of the sky-subtracted frames for each field/filter combination, using offsets derived by calculating the centroids of individual stars; and (5) construction of the final

TABLE 1

SUMMARY OF OBSERVATIONS

Field	R.A. (2000.0)	Decl. (2000.0)	R_{center} (core radii)[a]	Exposure Time (s)	FWHM
1.....	$18^h36^m23^s.9$	−23°54′12″	0.0	3 × 1(J)	0.″6
				3 × 1(K')	0.6
				3 × 10(J)	0.6
				3 × 10(K')	0.6
2.....	18 36 25.9	−23 52 26	1.5	3 × 60(J)	0.8
				3 × 60(K')	0.8
3.....	18 36 46.4	−23 58 27	5.5	12 × 120(J)	0.8
				12 × 120(K')	0.8
4.....	18 36 26.1	−23 23 45	25.3	9 × 120(J)	0.8
				9 × 120(K')	0.9

[a] Distance from cluster center, assuming a core radius of 72.″1 (Webbink 1985).

images, which was done by computing the median intensity at each pixel location in the aligned frames. Final K' images of all four fields are shown in Figure 1. The background noise levels in the upper left-hand quadrants of the field 3 and field 4 images are slightly higher than in the rest of these frames, a problem that was traced to the array controller and was corrected prior to recording the field 1 and field 2 data. Given that the photometric quality of faint sources is sensitive to detector noise, it was decided not to perform photometry on the affected portions of fields 3 and 4.

3. PHOTOMETRIC MEASUREMENTS AND THE $(K, J-K)$ CMD OF M22

The brightnesses of individual stars were measured with the point-spread function (PSF) fitting routine ALLSTAR (Stetson & Harris 1988), which is part of the DAOPHOT (Stetson 1987) photometry package. Completeness fractions and uncertainties in the measured brightnesses were determined from artificial star experiments, in which scaled versions of the PSFs were added to the reduced images. DAOPHOT and ALLSTAR were then run on these images and the artificial star recovery statistics computed. These experiments reveal that the 50% completeness levels in fields 2, 3, and 4 occur at $K = 16.5$, 19.0, and 18.5, respectively.

The $(K, J-K)$ diagrams for each field are shown in Figure 2. Only those stars with fitting errors, as computed by ALLSTAR, less than 0.07 mag in each bandpass have been included in these plots. M22 is one of the closest globular clusters and, in the absence of extreme crowding and reddening, there should be little difficulty in obtaining near-infrared photometry of stars at or below the brightness of the MSTO. This turns out to be the case—even the field 1 CMD, for which the total integration time was only 30 s per filter, extends as faint as the MSTO, while the CMDs of fields 2 and 3 include stars that are well below the MSTO. A blue horizontal branch (BHB) component is also evident in the field 1 CMD near $K \sim 13.5$ and $J-K \sim 0.1$.

Frogel, Persson, & Cohen (1983b, hereafter FPC) obtained infrared aperture photometry of 19 stars outside the central regions of M22. Stars with brightnesses similar to those studied by FPC were intentionally avoided in fields 2, 3, and 4 of the current study to prevent saturating the detector, so there is no chance of conducting a star-by-star comparison with the FPC results. Nevertheless, the 1 s field 1 exposures contain a number of bright stars that are not saturated, and the CMD constructed from these data are compared with the FPC photometry in Figure 3. The star I82, which FPC identified as a field object based on radial velocity measurements, was not included in this comparison, as were those stars that are confirmed variables. The

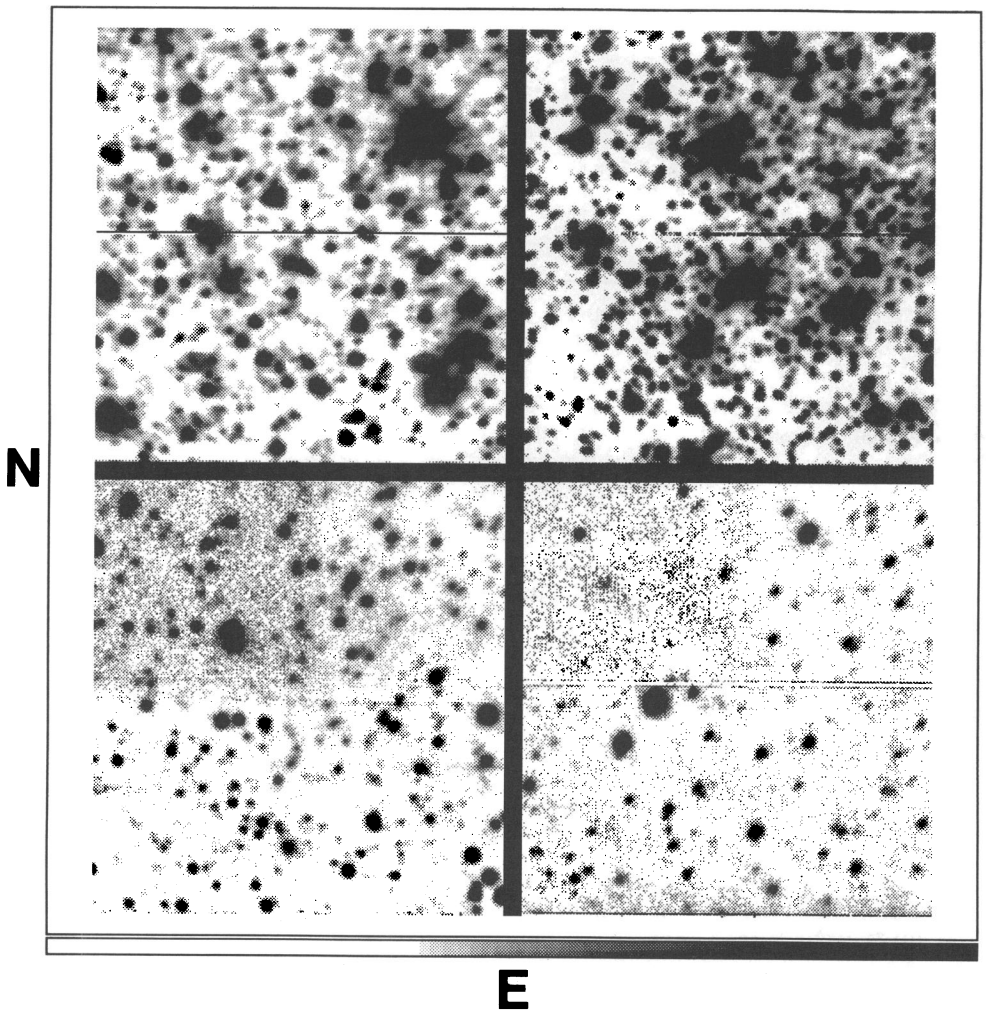

FIG. 1.—Final K images for fields 1, 2, 4, and 3 (*clockwise from upper left-hand corner*)

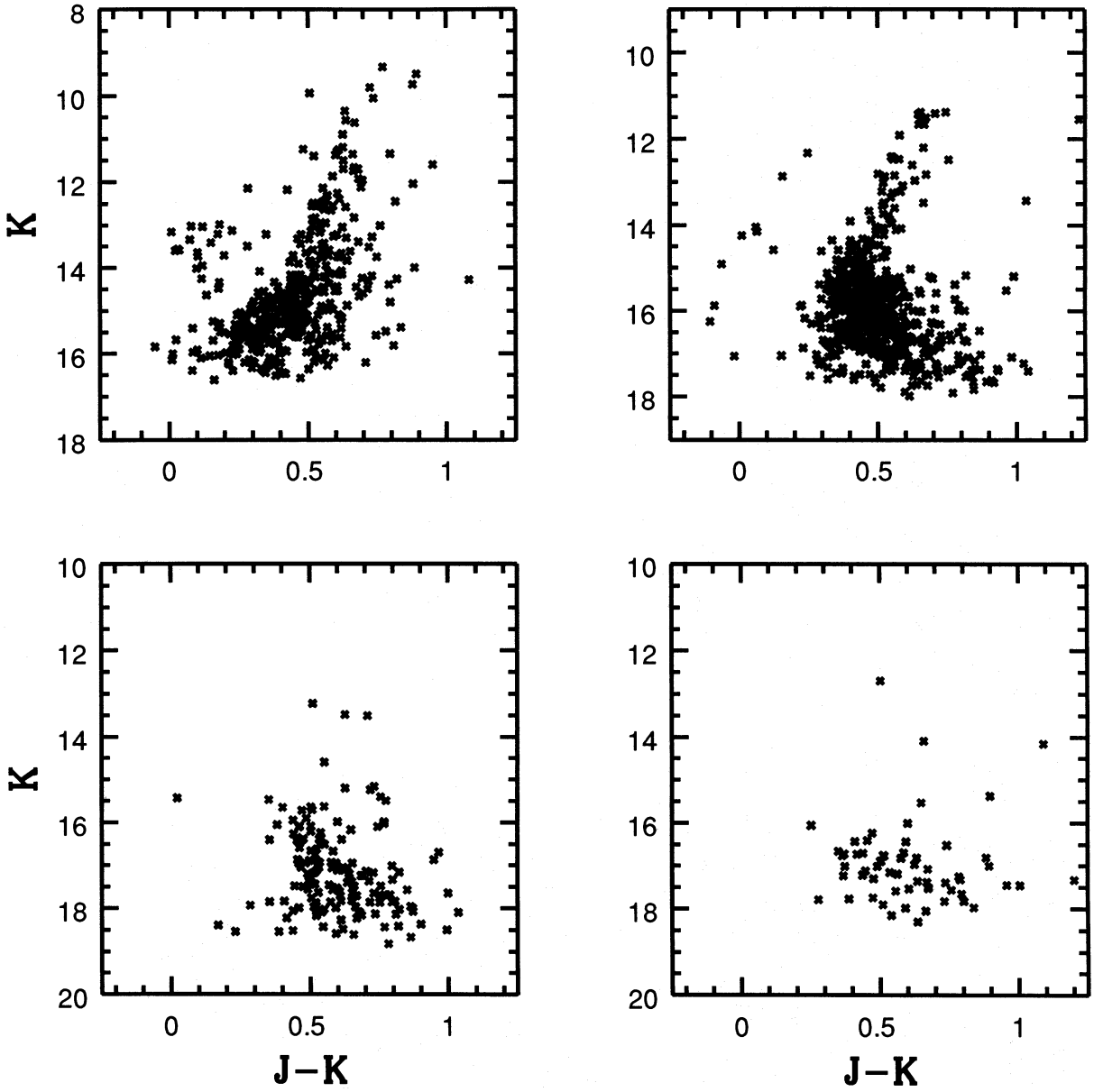

FIG. 2.—($K, J-K$) CMDs for fields 1, 2, 4, and 3 (*clockwise from upper left-hand corner*). The field 1 CMD is that produced from the 10 s exposures of this field. Only those stars with uncertainties, as estimated by ALLSTAR, in the measured brightnesses ≤ 0.07 mag are shown.

comparison in Figure 3 suggests that the color calibration of our data is consistent with that of the FPC aperture measurements.

The field 3 CMD samples the faintest stars in our data set; unfortunately, the number density of cluster stars is relatively low, amounting to only a factor of 2 or 3 above background. In an effort to highlight the cluster sequence in field 3, we used the field 4 CMD to correct statistically for field star contamination, and the result is shown in Figure 4. Background stars were removed by identifying those stars in field 3 that had locations on the CMD closest to stars in field 4. The field 3 stars matched in this fashion were then deleted from the CMD. While the M22 main sequence is evident in Figure 4, we caution that this technique assumes that fields 3 and 4 have similar reddenings, and any deviations from this condition will artificially broaden the cluster sequence in the background-subtracted CMD.

Normal points that trace the near-infrared CMD of M22 from the upper RGB to below the MSTO were computed to facilitate comparisons with other cluster sequences and theoretical isochrones. These were derived by grouping the CMD data in bins of width ± 0.25 mag in K, and then computing the mean $J-K$ color in each bin. An iterative 2 σ rejection criterion was applied to remove outliers. A narrower bin size of ± 0.125 mag in K was used in the vicinity of the MSTO, as color changes very rapidly with brightness in this part of the CMD. The field 1 data were combined with the aperture measurements made by FPC to define the upper RGB, while the field 1, 2, and 3 observations defined the subgiant branch (SGB), MSTO, and main-sequence components. The resulting normal points are listed in Table 2 and are plotted in Figure 5.

4. COMPARISONS WITH THEORETICAL ISOCHRONES

Comparisons between cluster CMDs and theoretical isochrones depend on a number of parameters, including age, reddening, chemical composition, and distance. To limit the number of free parameters, the distance, reddening, and

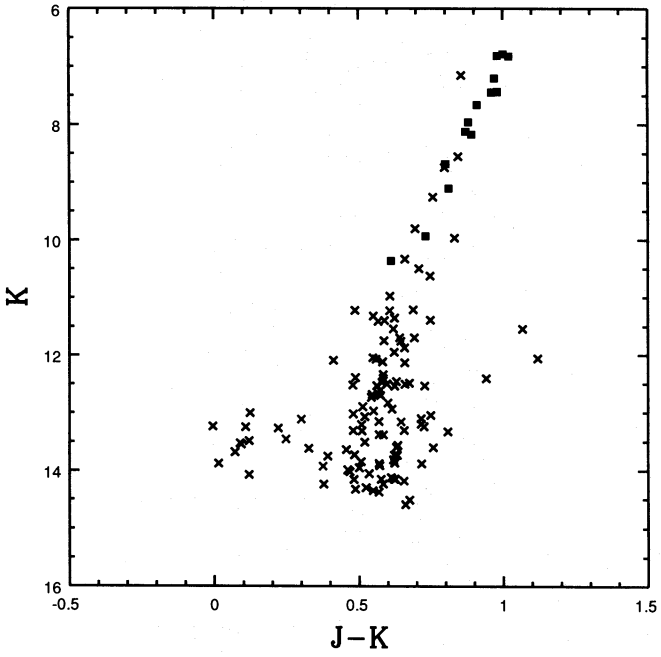

FIG. 3.—(K, $J-K$) CMD produced from the 1 s exposures of field 1 (*crosses*) compared with the aperture photometry measurements of selected M22 giants made by Frogel, Persson, & Cohen (1983b; *filled squares*). Note that the loci defined by these two data sets are in good agreement.

metallicity of M22 were fixed at the values listed in Table 3. $M_V^{HB} = 0.75$ (Carney, Storm, & Jones 1992) was adopted for computing the distance to M22, while the reddening curve of Rieke & Lebofsky (1985) was used to derive $E(J-K)$ and A_K.

The $B-V$ color excess listed in Table 3 is a weighted average of three estimates. Using photometric measurements in the Strömgren system, Hesser (1976) concluded that $E(B-V) = 0.32$, while, based on the integrated $B-V$ color of M22, Reed, Hesser, & Shawl (1988) found that $E(B-V) = 0.34$. More recently, Crocker (1988) measured

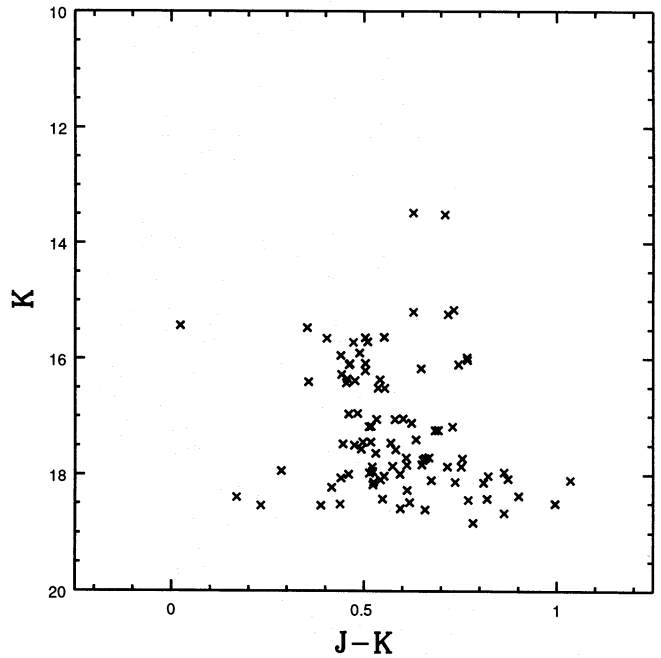

FIG. 4.—Background-corrected (K, $J-K$) CMD of field 3. See text for additional details.

TABLE 2

M22 NORMAL POINTS

K	$J-K$	K	$J-K$
7.00.....	0.99	14.00.....	0.53
7.50.....	0.94	14.25.....	0.48
8.00.....	0.89	14.50.....	0.45
8.50.....	0.84	14.75.....	0.43
9.00.....	0.80	15.00.....	0.42
9.50.....	0.76	15.25.....	0.42
10.00.....	0.72	15.50.....	0.43
10.50.....	0.69	15.75.....	0.45
11.00.....	0.64	16.00.....	0.47
11.50.....	0.62	16.25.....	0.49
12.00.....	0.60	16.50.....	0.51
12.50.....	0.57	17.00.....	0.56
13.00.....	0.55	17.50.....	0.62
13.50.....	0.54	18.00.....	0.68

the strengths of Balmer lines in cluster BHB stars and found that $E(B-V) = 0.42$. We consider this last result to be more reliable than the others, as it is based on stars that are likely cluster members whereas the other two estimates are prone to field star contamination. Therefore, when computing an average value of $E(B-V)$, the Crocker (1988) reddening value was assigned a weight twice that of the others.

A potential source of complication when defining [Fe/H] for M22 is that star-to-star metallicity variations may be present. Lehnert et al. (1991) measure an [Fe/H] dispersion in the range 0.2–0.3 dex, with [Fe/H] falling between −1.4 and −1.7, while Brown & Wallerstein (1992) conclude that CN weak and CN strong stars in M22 have [Fe/H] = −1.8 and −1.6, respectively. A metallicity dispersion will smear the giant branch on the CMD, so it may be possible to determine if an abundance spread is present using photometry. Unfortunately, the near-infrared photometric data

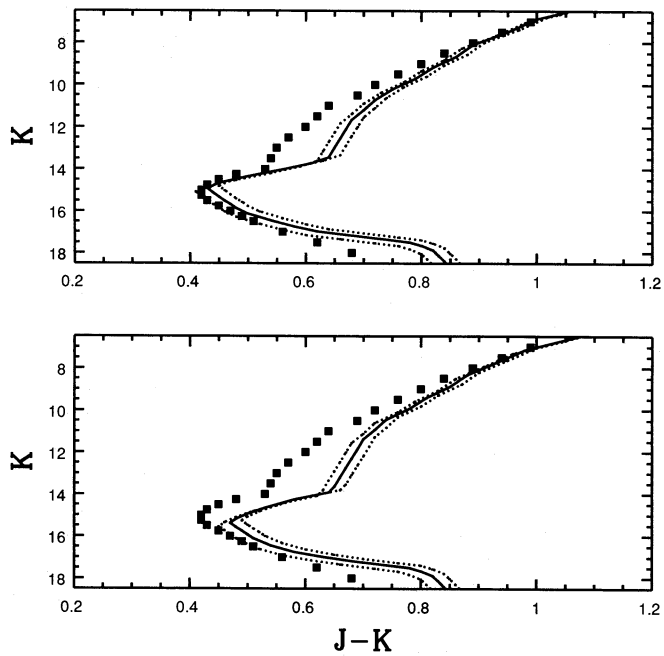

FIG. 5.—M22 normal points (*filled squares*) compared with the 12 (*upper panel*) and 16 Gyr (*lower panel*) [Fe/H] = −1.78 oxygen-enhanced isochrones of Bergsbusch & VandenBerg (1992). The solid line show the thoeretical isochrones if $E(B-V)_{M22} = 0.38$, while the dashed lines show the isochrones as they would appear with $E(B-V)_{M22} = 0.32$ and 0.42, which are the extremes quoted in the literature.

TABLE 3

ADOPTED PARAMETERS FOR M22 AND M13

Cluster	$E(B-V)$	V_{HB}	[Fe/H]
M22.....	0.38[a]	14.10[b]	−1.75[c]
M13.....	0.02[d]	14.95[d]	−1.65[c]

[a] See text.
[b] Peterson & Cudworth 1994.
[c] Zinn & West 1984.
[d] Armandroff 1989.

are not of sufficient quality to detect a metallicity dispersion of the size thought to be present in M22. Using the calibration between [Fe/H] and $J-K$ color at $M_K = -5.5$ from Figure 3 of Frogel, Cohen, & Persson (1983a, hereafter FCP), a metallicity dispersion of 0.25 dex should broaden the upper giant branch by ~ 0.04 mag in $J-K$. Unfortunately, this is comparable to the smearing introduced by variations in $E(B-V)$. Moreover, the artificial star experiments, described in § 3, indicate the the photometric errors in field 1 are roughly ± 0.07 mag for upper giant branch stars, so the scatter in the current CMD is dominated by photometric uncertainties.

For the present study, we adopt the metallicity computed by Zinn & West (1984), who used a number of different indicators to assign M22 [Fe/H] = −1.75. Although falling near the upper range of values derived from recent spectroscopic work, this metallicity is consistent with that computed for CN-weak stars in M22 (see Brown & Wallerstein 1992), which appear to be the most common star in the cluster. In any event, we emphasize that the basic findings of this section are relatively insensitive to the adopted mean metallicity; for example, our basic conclusions would not change if [Fe/H] = −1.65 were adopted instead.

The M22 normal points were compared with near-infrared isochrones constructed using the procedures described in Paper III. Selected (M_V, $B-V$) pairs from the optical sequences tabulated by Bergbusch & VandenBerg (1992) and Straniero & Chieffi (1991) were transformed into corresponding (M_K, $J-K$) values using relations among $B-V$, $V-K$, and $J-K$ derived from metal-poor dwarfs and giants. As noted in Paper III, these color relations do not include the SGB and lower RGB, so these particular evolutionary phases were transformed onto the near-infrared plane with the aid of synthetic near-infrared brightnesses and colors computed by Bell (1992) and Bell & Gustafsson (1989). Bell (1992) and Davidge & Simons (1994a, b) found that these synthetic near-infrared measurements contain calibration errors which depend on both surface gravity and effective temperature, and the following procedure was used to compensate for these. To start, the offsets required to splice the transformed SGB and lower RGB sequences onto those portions of the isochrones derived from the empirical color relations were computed. The offset required to match the SGB to the MSTO were slightly different from those needed to produce a continuous RGB. Therefore, to prevent introducing discontinuities in the isochrones, the offsets applied to intermediate points were computed by interpolating with respect to surface gravity between the SGB and lower RGB offsets.

The 12 and 16 Gyr [Fe/H] = −1.78 oxygen-enhanced Bergbusch & VandenBerg (1992) isochrones are compared with the M22 normal points in Figure 5. The dashed lines in Figure 5 show the isochrones as they would appear if $E(B-V)_{M22} = 0.32$ and 0.42 were adopted, and it is evident that the effects of reddening are greatest on the lower RGB and the main sequence below the turnoff. For comparison, the brightnesses of the MSTO and the SGB are relatively insensitive to $E(B-V)$.

The models with $E(B-V) = 0.38$ fall slightly redward of the M22 sequence, and the size of this discrepancy depends on isochrone age. Uncertainties in reddening notwithstanding, both the 12 and 16 Gyr isochrones provide a reasonable match to the color of the main sequence below the turnoff as well as the upper portions of the RGB. However, the lower portions of the RGB are not well matched by the models, a point that will be discussed further in § 5. Perhaps the most significant finding from Figure 5 is that only the 12 Gyr isochrone is able to match the brightnesses of the MSTO and SGB in M22—the 16 Gyr isochrone predicts brightnesses for the MSTO and SGB that are roughly 0.5 mag too faint. These differences are substantially larger than the uncertainties in the photometric calibration, so we conclude that the 16 Gyr isochrone provides an unacceptable match to the data.

The Bergbusch & VandenBerg (1992) models assume that [O/Fe] = 0.66, which is larger than what has been measured in M22 giants (e.g., Brown et al. 1990). Isochrone morphology is sensitive to element mixtures (e.g., VandenBerg & Stetson 1991), so it is of interest to compare the M22 CMD with models that make different assumptions for chemical mixture. Therefore, we have also compared the M22 normal points with the 12 and 16 Gyr $z = 0.0003$ (i.e., [Fe/H] = −1.75) models of Straneiro & Chieffi (1991), which are based on scaled solar chemical mixtures (i.e., [O/Fe] = 0), and the results are given in Figure 6, where the dashed lines show the isochrones as they would appear for extreme values of $E(B-V)$. As was seen in Figure 5, there is

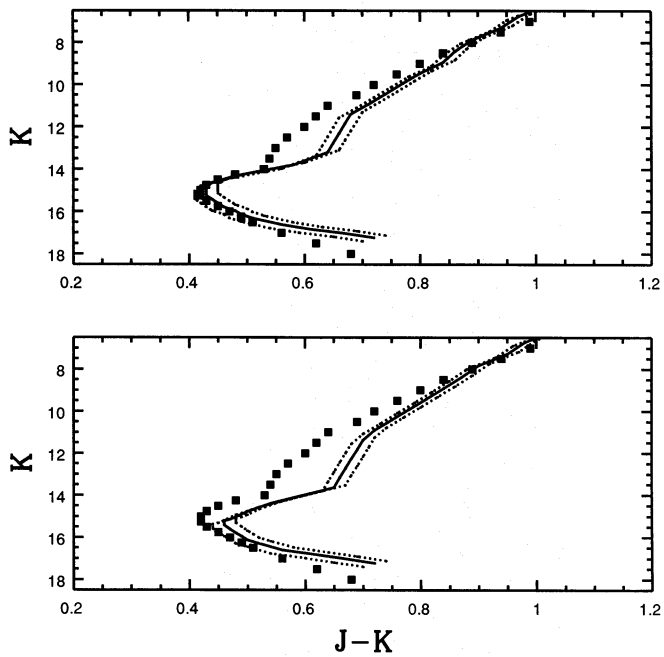

FIG. 6.—M22 normal points (*filled squares*) compared with 12 (*upper panel*) and 16 Gyr (*lower panel*) $z = 0.0003$ (i.e., [Fe/H] ~ −1.75) solar mixture isochrones of Straniero & Chieffi (1991). The solid lines show the thoeretical isochrones if $E(B-V)_{M22} = 0.38$, while the dashed lines show the isochrones as they would appear with $E(B-V)_{M22} = 0.32$ and 0.42.

a tendency for the models with $E(B-V) = 0.38$ to fall slightly redward of the M22 sequence, although the discrepancy for the 12 Gyr model is small. Moreover, once again the 12 Gyr model provides a good match to the MSTO region, while the 16 Gyr sequence does not. Finally, we note that the Straniero & Chieffi models do not fit the upper RGB of M22 as well as they fit the Bergbusch & VandenBerg (1992) sequences.

5. COMPARISONS WITH M13

The comparisons with near-infrared isochrones in § 4 suggest that M22 has an age near 12 Gyr, independent of chemical mixture. However, we caution that this age estimate is highly uncertain, as our knowledge of stellar structure still contains significant gaps (e.g., VandenBerg 1992). It has been suggested that the direct comparison of observed CMDs may provide a means of deriving *relative* cluster ages (e.g., VandenBerg, Bolte, & Stetson 1990; Sarajedini & Demarque 1990) free of the uncertainties associated with stellar models. While this is true in principle, such an approach does not provide an unambiguous means of ranking cluster ages in practice, as a tacit assumption is that the chemical compositions of the clusters being compared are not significantly different. In this section we compare the M22 normal points with those derived in Paper III for M13.

The M22 and M13 near-infrared sequences are compared in the upper panel of Figure 7, where the dotted lines show the effects of adopting $E(B-V) = 0.32$ and 0.42. The M13 data in the upper panel of Figure 7 have been shifted to match the distance and reddening of M22 using the HB brightnesses and reddenings summarized in Table 3. That is, aside from minor corrections to account for differences in [Fe/H] (see below), the HB luminosities of both clusters are implicitly the same for this comparison.

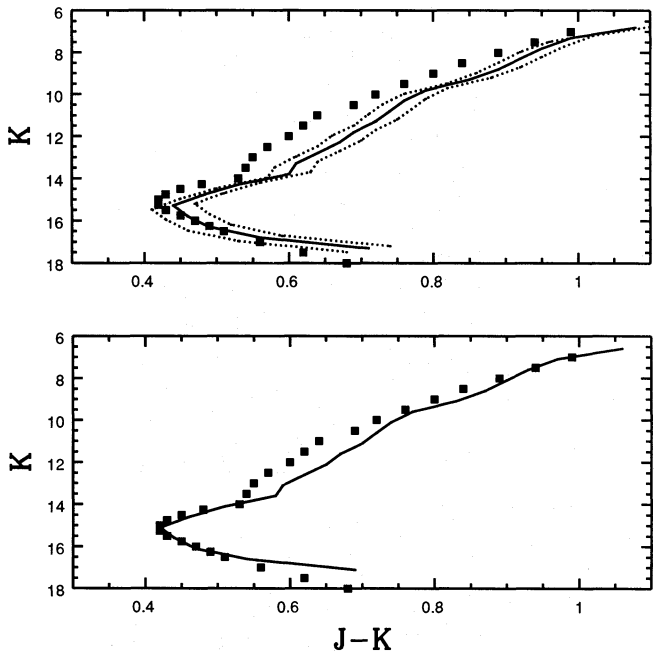

FIG. 7.—M22 normal points (*filled squares*) compared with the ridgeline derived for M13 by Davidge & Harris (1995; *solid line*). In the top panel, the M13 sequence is shown as it would appear if shifted to compensate for differences in distance, reddening, and metallicity with $E(B-V)_{M22} = 0.38$. The dashed lines in this panel show the M13 sequence as it would appear if $E(B-V)_{M22} = 0.32$ and 0.42. In the lower panel, the M13 sequence has been shifted to match the M22 CMD in the vicinity of the MSTO. Note that the lower giant branch of M22 falls well blueward of the M13 sequence, although the cluster ridgelines are coincident on the upper giant branch.

The metallicity adopted for M22 in Table 3 is slightly lower than that of M13, so two metallicity-dependent corrections were applied to the M13 sequence. First, there is growing observational and theoretical evidence that the brightness of the HB depends on metallicity, and we have assumed that HB stars in M13 are intrinsically brighter than those in M22 by an amount $\Delta M_V^{HB}/\Delta[Fe/H] = 0.15$ (Carney et al. 1992). Second, if M13 is slightly more metal-rich than M22, then, after correcting for differences in distance and reddening, the M13 sequence should fall slightly redward of M22. The offset expected between the cluster giant branches can be estimated from the relation between giant branch color and [Fe/H] shown in Figure 3 of FCP. According to this relation, if $[Fe/H]_{M22} = -1.75$ and $[Fe/H]_{M13} = -1.65$, then the M13 giant branch should have $J-K$ colors that are 0.02 mag redder than M22. An offset of this size was applied to the M13 data in Figure 7 to correct for this effect, although it is worth noting that if stars in M13 and M22 have different values of [O/Fe], then a luminosity-sensitive metallicity correction would be more appropriate (e.g., VandenBerg & Stetson 1991).

It is evident from the upper panel of Figure 7 that the main sequences of M22 and M13 are in fair agreement. The agreement in the vicinity of the MSTO is not perfect, in that the M13 MSTO is redder than that of M22 by ~0.02–0.03 mag. However, this difference is likely not significant, as it is within the uncertainty in the photometric zero points (Paper III) and the adopted reddenings, while the CMDs can be well matched in the vicinity of the MSTO if modest color and brightness shifts are applied to the M13 data. To demonstrate this, following the basic procedure outlined by VandenBerg et al. (1990), horizontal and vertical shifts were applied to the M13 data such that the MSTO colors and the main-sequence brightness 0.05 mag redward of the MSTO were aligned, and the result is shown in the lower panel of Figure 7.

The color difference between the MSTO and the base of the RGB is a criterion that VandenBerg et al. (1990) and Sarajedini & Demarque (1990) have used to rank cluster ages. It is apparent from the lower panel of Figure 7 that the lower RGB in M22 falls well blueward of M13, ostensibly suggesting that M22 is considerably older than M13. However, there are three pieces of evidence that run counter to this interpretation. First, if M13 were younger than M22, then the color difference should extend over the entire giant branch, and this is not the case, since the M13 and M22 sequences overlap on the upper RGB. Second, if M13 were younger than M22, then the MSTO in this cluster should be brighter than that in M22, and the comparison in the upper panel of Figure 7 shows that this is not the case. Indeed, in order to shift the M13 sequence to match that of M22 in the lower panel of Figure 7, it was necessary to apply an offset of 0.2 mag to the M13 sequence along the vertical axis, in the sense of making these data *brighter*. Finally, the distribution of stars on the HB is sensitive to age, and M13 and M22 have very similar values of the HB morphology parameter $(B-R)/(B+V+R)$ (Lee 1990). Consequently, we suspect that M22 is *not* older than M13.

At this point it is worth noting that it has long been suspected that the photometric properties of the M22 giant

branch are anomalous. Indeed, Hesser et al. (1977) concluded that the slope of the giant branch in the optical CMD was shallower than in other clusters of similar metallicity. This is clearly evident in Figure 7: whereas the M13 and M22 sequences show good agreement on the upper giant branch, the lower giant branches differ by ~ 0.05 mag in $J-K$. The Hesser et al. (1977) study relied on a modest number of observations, which showed considerable scatter and covered only the upper giant branch, so it is important to determine whether larger optical data sets, spanning the entire RGB, verify these results. Therefore, we have compared the giant branch sequences of M13 and M22 on the $(V, B-V)$-plane using recent data from the literature, and the results are shown in Figure 8. The basis for this comparison are ridgelines which were derived by tracing the loci of the $(V, B-V)$ CMDs by hand. The M22 sequence was constructed from CMDs given by Peterson & Cudworth (1994) for $V \leq 14$ and Samus et al. (1995) for $V \geq 14$ (note that these two data sets show excellent agreement in the region of overlap, so it was not necessary to apply color offsets to produce a continuous giant branch). The M13 sequence was constructed from the CMDs given by Guarnieri, Bragaglia, & Fusi Pecci (1993). The M13 sequence was shifted to match the distance and reddening of M22. Moreover, the M13 data were offset by 0.02 mag to lower $B-V$ values to compensate for the difference in metallicity between the two clusters, a correction factor derived from the Straniero & Chieffi (1991) isochrones.

The M22 and M13 giant branches in Figure 8 show differences reminsicent of those in the upper panel of Figure 7. In particular, at intermediate brightnesses the M22 sequence falls blueward of M13, and there is a tendency for the two giant branches to merge near the RGB tip. The mean color difference between the giant branches in Figure 8 is sensitive to the adopted reddening of M22, and the extent of this dependence is shown by the dotted lines, which hold for $E(B-V) = 0.32$ and 0.42. The M22 and M13 giant branches are coincident if $E(B-V)_{M22} = 0.32$. However, this then produces an inconsistency with the infrared photometry; if $E(B-V)$ were this low, then, based on the comparison in the upper panel of Figure 7, the difference in K brightness between the MSTOs of M13 and M22 would be almost 0.4 mag, indicating an age difference between M22 and M13 of almost 4 Gyr, with M22 the younger. In this case the problem presented by the color difference between the MSTO and the base of the RGB in Figure 7 is exacerbated. The positions of the SGBs in Figure 8 are also of potential interest, and it may be worth noting that there is good agreement between the M13 and M22 SGBs if $E(B-V)_{M22} = 0.38$. Unfortunately, the significance of this result is low, as the SGB for M22 in the Samus et al. (1995) photometry shows substantial scatter in $B-V$, and falls near the plate limit. Clearly, it would be highly desirable to obtain short-exposure CCD images of both clusters to better define the SGB sequences.

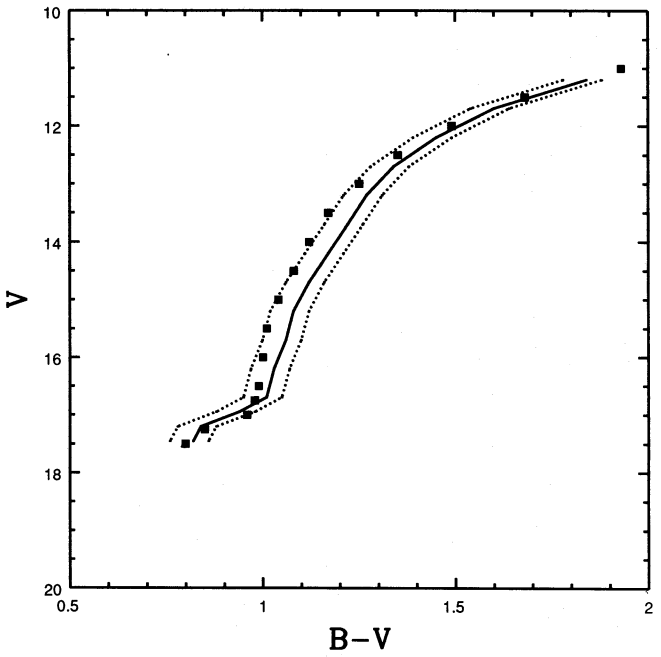

FIG. 8.—Ridgeline of the M22 giant branch derived from $(V, B-V)$ observations (*filled squares*) compared with that for M13. The solid line shows the M13 sequence shifted to compensate for differences in distance, reddening, and metallicity if $E(B-V)_{M22} = 0.38$. The dashed lines show the M13 sequence if $E(B-V)_{M22} = 0.32$ and 0.42. See text for additional details.

A better match between the giant branch loci of M13 and M22 in the upper panels of Figures 7 and 8 would result if the metallicity difference between these clusters had been *underestimated*; in particular, if the difference in [Fe/H] was 0.2 dex, rather than 0.1 dex, then the metallicity color correction applied to M13 should be larger, and the two giant branches would be better aligned (although the discrepancy between the overall slopes of the giant branches would remain). Metallicity estimates for globular clusters are usually based on a number of techniques, and slight differences in the calibrations of these may exist. As a result, the relative metallicities of clusters could be uncertain if different techniques were used to estimate [Fe/H]. In an effort to produce internally homogeneous [Fe/H] measurements for M22 and M13, we derived metallicities using only those entries in Table 5 of Zinn & West (1984) that are common to both clusters, these being $[Fe/H]_C$, $[Fe/H]_{IR}$, $[Fe/H]_{T_e}$, $[Fe/H]_{RGB}$, $[Fe/H]_{\Delta V}$, and $[Fe/H]_{Q39}$. Based on these six methods, we find that $[Fe/H]_{M13} = -1.58$ and $[Fe/H]_{M22} = -1.70$. Hence, $\Delta[Fe/H] = 0.12$, which is very close to the difference of 0.1 dex resulting from our adopted values of [Fe/H] in Table 3. The study conducted by Lehnert et al. (1991), who recorded spectroscopic observations of 10 stars in each cluster, provides further support that the difference in metallicity between M22 and M13 has not been underestimated, as these authors conclude that $\Delta[Fe/H] = 0$.

Why does the color difference between the MSTO and the lower giant branch in M22 not provide an accurate means of gauging age with respect to M13? Detailed comparative spectroscopic investigations of main-sequence and evolved stars in M22 and M13 will undoubtedly provide important clues for answering this question. Nevertheless, existing data sets provide tantalizing hints as to possible causes. For example, the majority of giants in M13 are oxygen deficient (Kraft et al. 1993), while there appears to be a significant number of oxygen-enhanced stars in M22 (Brown et al. 1990). There are indications that this difference in chemical mixture does not extend to all α-elements, as Lehnert et al. (1991) find similar [Ca/Fe] values in M13 and M22. The question of α-element abundance is significant, since if only certain elements, such as oxygen, are enhanced, then the location of the giant branch locus with respect to

the MSTO may be affected (VandenBerg & Stetson 1991); on the other hand, if all α-elements are enhanced by similar amounts, then the net effect will be like that of a bulk increase in [Fe/H] (Salaris, Chieffi, & Straniero 1993). The general sense of the differences in [O/Fe] between M22 and M13 is *qualitatively* consistent with the relative locations of the giant branches *at intermediate brightnesses*. However, there are problems attributing the relative giant branch locations to [O/Fe]. First, the models generated by VandenBerg & Stetson (1991) predict that the giant branches should run parallel over the entire range of brightnesses, and not merge near the RGB tip. Second, the VandenBerg & Stetson (1991) models predict that a 0.04 difference in $J-K$, which is what is seen near the RGB tip in the upper panel of Figure 7, requires Δ[O/Fe] ~ 1.5 if $\Delta(J-K)/\Delta(B-V) = 0.62$ for metal-poor giants (Davidge & Simons 1994a), and this difference in [O/Fe] is much larger than what has been measured spectroscopically.

The RGB temperature is also sensitive to other, considerably less well understood, factors such as the presence of binaries (large numbers of them would shift the mean RGB color blueward, particularly on the low-luminosity end), mass loss during the giant stage (or differential mass loss), and stellar rotation. Any or all of these may differ between M13 and M22, as well as the detailed chemical composition factors already mentioned; but at present these options must remain highly speculative.

6. THE LUMINOSITY AND MASS FUNCTIONS OF M22

Djorgovski, Piotto, & Capaccioli (1993) investigated the relation between globular cluster mass function exponent and parameters such as chemical composition and location

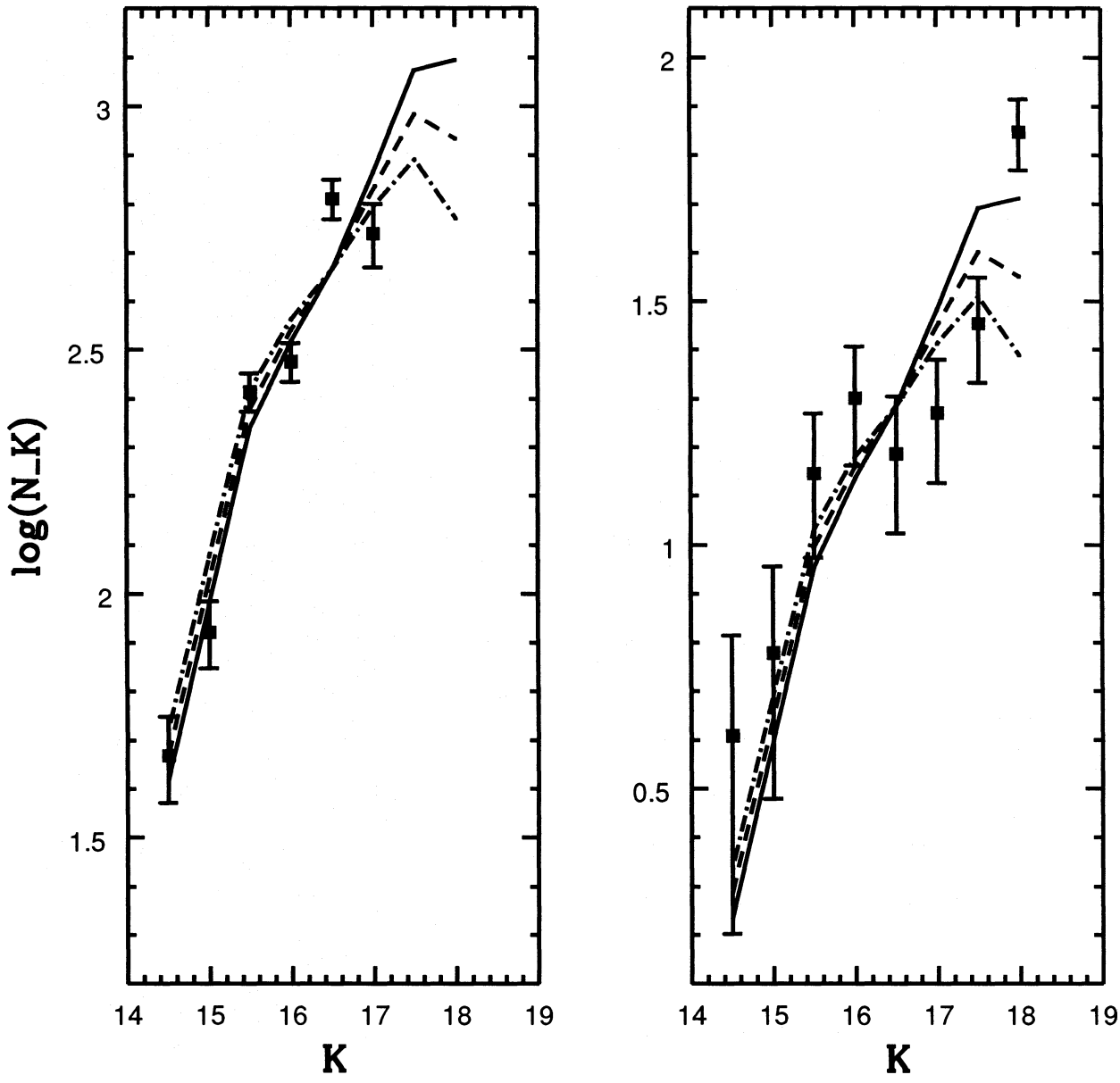

FIG. 9.—K luminosity functions for fields 2 (*left-handed panel*) and 3 (*right-hand panel*), corrected for incompleteness and background contamination. The error bars reflect counting statistics. N_K is the number of stars per 0.5 mag interval per square arcminute. Also shown are model luminosity functions derived from the 12 Gyr [Fe/H] $= -1.78$ isochrones of Bergsbusch & VandenBerg (1992) for three mass function exponents: $x = -1$ (*solid line*), 0 (*dashed line*), and $+1$ (*dash-dotted line*). The models have been scaled to match the observed number of stars between $K = 14.5$ and 17. Note that the theoretical curves only diverge significantly when $K \geq 17$.

in the Galaxy. After performing a principal component analysis, they conclude that the mass function exponent in the interval 0.5–0.8 $M_\odot$ depends on [Fe/H] and location in the Galaxy, as measured by distance from the Galactic center and height above the disk. Low-latitude clusters like M22, which fall within the solar circle, provide an important means of testing these trends, and in this section the near-infrared luminosity and mass functions of main-sequence stars in fields 2 and 3 are examined.

Corrections for sample incompleteness were derived from the artificial star experiments described in § 3, and these were applied to the data prior to the removal of field star contamination, which was accomplished by subtracting the completeness-corrected field 4 luminosity function. Furthermore, in an effort to prevent the inclusion of spurious objects, only those stars detected in both J and K' were used in this analysis. The resulting K luminosity functions, plotted in Figure 9, show increasing stellar density toward fainter brightness.

Theoretical luminosity functions were constructed from stellar evolution models for comparison with the observations. Mass funcions of the form $n\,dm = m^{-x}\,dm$ with $x = -1$, 0, and $+1$ were considered. The model luminosity functions constructed from the 12 Gyr [Fe/H] $= -1.78$ Bergsbusch & VandenBerg (1992) isochrone are compared with the field 2 and field 3 observations in Figure 9. The models, which have been scaled to match the observed number of stars in each field between $K = 14.5$ and 17.0, reproduce the general trends in the observations. Unfortunately, the models only diverge significantly when $K \geq 17$, and the scatter in the observations at these brightnesses is sufficiently large that only loose constraints can be placed on x.

Additional insight into the mass function may be gained by using the mass-brightness relations predicted from theoretical models to convert the observed luminosity functions into mass functions. For the current study, we use the mass-brightness relation derived from the 12 Gyr [Fe/H] $= -1.78$ Bergsbusch & VandenBerg (1992) isochrone, and the results for fields 2 and 3 are shown in Figure 10. The field 2 data sample a very limited range of masses, so no attempt was made to measure x from these data. However, the field 3 data extend down to 0.6 $M_\odot$, and a least-squares fit reveals that $x = -0.4 \pm 1.0$ if all data points are used.

Is the mass function exponent consistent with the trends defined by Djorgovski et al. (1993)? Based on equation (4) from that study, if $R_{GC}^{M22} = 5.1$ kpc, $Z_{GP}^{M22} = 0.4$ kpc, and [Fe/H] $= -1.8$, then the mass function in M22 should have an exponent $x \sim 0.5$. This is consistent within the errors of what is seen in field 3. Clearly it would be worthwhile to obtain deeper images of M22 in order to extend the observations to 0.5 $M_\odot$, and hence cover the entire range of masses considered by Djorgovski et al. (1993).

7. SUMMARY

We have presented the first CMD of M22 to sample stars fainter than the MTSO. After adopting canonical values for distance and reddening, the near-infrared brightness of the MSTO is found to be well matched by the 12 Gyr [Fe/H] $= -1.7$ isochrones of Berbsbusch & VandenBerg (1992) and Straniero & Chieffi (1991), which were transformed onto the near-infrared observational plane using techniques described in Paper III. For comparison, 16 Gyr models predict a MSTO that is much fainter and redder than that observed.

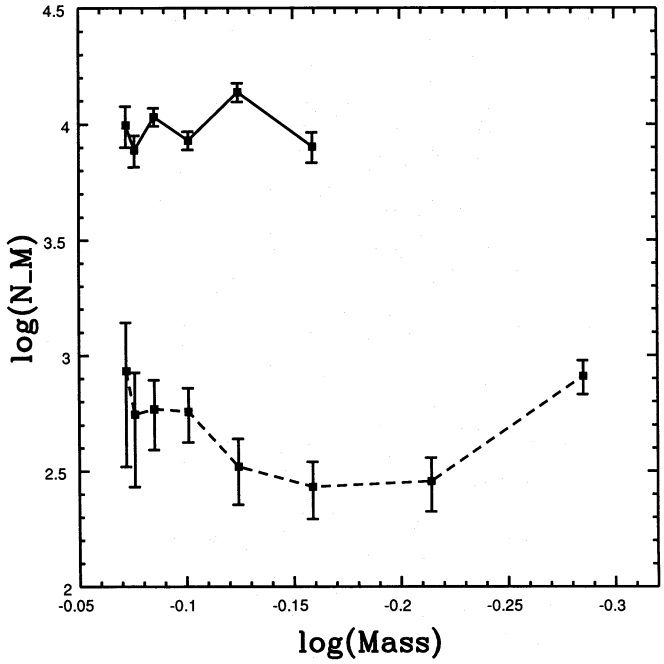

FIG. 10.—Mass functions for fields 2 (*upper curve*) and 3 (*lower curve*), as derived from the 12 Gyr [Fe/H] $= -1.78$ isochrone of Bergsbusch & VandenBerg (1992). N_M is the number of stars per solar mass per square arcminute. The error bars reflect counting errors.

The near-infrared M22 sequence has also been compared with that of M13. After correcting for differences in distance, reddening, and [Fe/H], the K brightnesses of the MSTO and SGB in M22 are found not to differ significantly from M13. However, the CMDs of these clusters are very different on the lower RGB, in the sense that the color difference between the MSTO and the base of the giant branch in M22 is much smaller than in M13. This difference does not extend over the entire giant branch; indeed, if the near-infrared CMDs of these clusters are shifted to align the MSTO region, then the upper RGB loci coincide. We suggest that a parameter (or parameters) other than age and [Fe/H] influences the location of the lower giant branch loci at near-infrared wavelengths. One implication is that it may be advisable to use the entire RGB sequence when using comparative techniques, such as those proposed by VandenBerg et al. (1990) and Sarajedini & Demarque (1990), to judge relative cluster ages. It would be highly useful to obtain near-infrared spectra of lower RGB stars in both clusters, as data of this nature may provide clues as to the source of the differences between the M22 and M13 giant branches.

Finally, we also investigated the luminosity and mass functions of M22. The luminosity functions of fields 2 and 3 are well matched by theoretical sequences, and the mass function exponent for field 3 is consistent with that predicted from statistical trends defined by other clusters.

The authors thank the Canadian Time Allocation Committee for granting observing time for this project. W. E. H. is supported by a research grant from the Natural Sciences and Engineering Research Council of Canada (NSERC). T. J. D. also extends thanks to the NSERC and the National Research Council of Canada for financial and infrastructure support.

REFERENCES

Alcaino, G. 1977, A&AS, 29, 383
Alcaino, G., & Liller, W. 1983, AJ, 88, 1330
Anthony-Twarog, B. J. Twarog, B. A., & Craig, J. 1995, PASP, 107, 32
Armandroff, T. E. 1989, AJ, 97, 375
Arp, H. C., & Melbourne, W. G. 1959, AJ, 64, 28
Bell, R. A. 1992, MNRAS, 257, 423
Bell, R. A., & Gustafsson, B. 1989, MNRAS, 236, 653
Bergbusch, P. A., & VandenBerg, D. A. 1992, ApJS, 81, 163
Brown, J. A., & Wallerstein, G. 1992, AJ, 104, 1818
Brown, J. A., Wallerstein, G., & Oke, J. B. 1990, AJ, 100, 1561
Carney, B. W., Storm, J., & Jones, R. V. 1992, ApJ, 386, 663
Casali, M., & Hawarden, T. 1992, JCMT-UKIRT Newsletter, 4, 33
Crocker, D. A. 1988, AJ, 96, 1649
Davidge, T. J., & Harris, W. E. 1995, ApJ, 445, 211 (Paper III)
Davidge, T. J., & Simons, D. A. 1994a, ApJ, 423, 640
———. 1994b, ApJ, 435, 207
Djorgovski, S., Piotto, G., & Capaccioli, M. 1993, AJ, 105, 2148
Fried, D. L. 1966, J. Opt. Soc. AM., 56, 1372
Frogel, J. A., Cohen, J. G., & Persson, S. E. 1983a, ApJ, 275, 773 (FCP)
Frogel, J. A., Persson, S. E., & Cohen, J. G. 1983b, ApJS, 53, 713 (FPC)
Guarnieri, M. D., Bragaglia, A., & Fusi Pecci, F. 1993, A&AS, 102, 397
Hesser, J. E. 1976, PASP, 88, 849
Hesser, J. E., Hartwick, F. D. A., & McClure, R. D. 1976, ApJ, 207, L113
———. 1977, ApJS, 33, 471
Kraft, R. P., Sneden, C., Langer, G. E., & Shetrone, M. D. 1993, AJ, 106, 1490
Langer, G. E., Hoffman, R., & Sneden, C. 1993, PASP, 105, 301
Lee, Y.-W. 1990, ApJ, 363, 159
Lehnert, M. D., Bell, R. A., & Cohen, J. G. 1991, ApJ, 367, 514
Lloyd Evans, T. 1975, MNRAS, 171, 647
———. 1978, MNRAS, 182, 293
Norris, J., & Freeman, K. C. 1983, ApJ, 266, 130
Peterson, R. C., & Cudworth, K. M. 1994, ApJ, 420, 612
Reed, B. C., Hesser, J. E., & Shawl, S. J. 1988, PASP, 100, 545
Rieke, G. H., & Lebofsky, M. J. 1985, ApJ, 288, 618
Salaris, M., Chieffi, A., & Straniero, O. 1993, ApJ, 414, 580
Samus, N., Kravtsov, V., Pavlov, M., Alcaino, G., & Liller, W. 1995, A&AS, 109, 487
Sarajedini, A., & Demarque, P. 1990, ApJ, 365, 219
Simons, D. A., Clark, C. C., Massey, S., Smith, S., & Toomey, D. 1993, Proc. SPIE, 1946, 502
Smith, V. V., & Suntzeff, N. B. 1989, AJ, 97, 1699
Stetson, P. B. 1987, PASP, 99, 191
Stetson, P. B., & Harris, W. E. 1988, AJ, 96, 909
Straniero, O., & Chieffi, A. 1991, ApJS, 76, 525
VandenBerg, D. A. 1992, ApJ, 391, 685
VandenBerg, D. A., Bolte, M., & Stetson, P. B. 1990, AJ, 100, 445
VandenBerg, D. A., & Stetson, P. B. 1991, AJ, 102, 1043
Wainscoat, R. J., & Cowie, L. L. 1992, AJ, 103, 332
Wallerstein, G., Leep, E. M., & Oke, J. B. 1987, AJ, 93, 1137
Webbink, R. F. 1985, in IAU Symp. 113, Dynamics of Star Clusters, ed. J. Goodman & P. Hut (Dordrecht: Reidel), 541
Zinn, R., & West, M. J. 1984, ApJS, 55, 45